LAWRENCE
LIVERMORE
NATIONAL
LABORATORY

LLNL-JRNL-406419

Sensitivity of NIF-scale backlit thin shell implosions to hohlraum symmetry in the foot of the ignition drive pulse

R. K. Kirkwood, J. Milovich, D. K. Bradley, M. Schmitt, S. R. Goldman, D. H. Kalantar, D. Meeker, O. S. Jones, S. M. Pollaine, P. A. Amendt, E. Dewald, J. Edwards, O. L. Landen, A. Nikroo

August 20, 2008

Physics of Plasmas

Disclaimer

Sensitivity of NIF-scale backlit thin shell implosions to hohlraum symmetry in the foot of the ignition drive pulse

R.K. Kirkwood, J. Milovich, D.K. Bradley, M. Schmitt*, S. R. Goldman*, D.H. Kalantar, D. Meeker, O.S. Jones, S.M. Pollaine, P.A. Amendt, E. Dewald, J. Edwards, O.L. Landen, A. Nikroo#

Lawrence Livermore National Laboratory

*Los Alamos National Laboratory

#General Atomics

Abstract

A necessary condition for igniting indirectly-driven inertial confinement fusion (ICF) spherical capsules on the National Ignition Facility (NIF) is controlling drive flux asymmetry to the 1% level time-integrated over the pulse and with < 10%/ns swings during the pulse [J. D. Lindl *et al*., "The Physics Basis for Ignition using Indirect Drive Targets on the National Ignition Facility," Physics of Plasmas **11**, 339 (2003)]. While drive symmetry during the first 2 ns of the pulse can be inferred by using the re-emission pattern from a surrogate high Z sphere [E. Dewald et al. to be published in Rev. Sci. Inst.] and symmetry during the last 5 ns inferred from the shape of fully imploded capsules [A. Hauer, N. Delamater, D. Ress *et al*. Rev. Sci. Instrum. **66**, 672-7 (1995)], the mid-portion (≈ 2-10 ns) has been shown to be amenable to detection by the in-flight shape of x-ray backlit thin shell capsules [Pollaine et. al., Physics of Plasmas **8** 2357 (2001)]. In

this paper, we present sensitivity studies conducted on the University of Rochester's OMEGA laser of the thin shell symmetry measurement technique at near NIF-scale for two candidate capsule ablator materials, Ge-doped CH and Cu-doped Be. These experiments use both point and area backlighting to cast 4.7 keV radiographs of thin 1.4 mm initial-diameter Ge-doped CH and Cu-doped Be shells when converged a factor of ≈ 0.5 x in radius. Distortions in the position of the transmission limb of the shells resulting from drive asymmetries are measured to an accuracy of a few μms, meeting requirements. The promising results to date allow us to compare measured and predicted distortions and by inference drive asymmetries for the first 4 asymmetry modes as a function of hohlraum illumination conditions.

I. Introduction

The National Ignition Facility (NIF) is a 192 beam, 1.8 MJ 0.35 μm laser now being built at Lawrence Livermore National Laboratory [1]. NIF is designed to drive inertial confinement fusion (ICF) capsules to ignition initially using indirect drive, in which the laser energy is converted to thermal x rays inside a cavity (hohlraum). The x rays then ablate the outer layers of a capsule inside the hohlraum, causing the capsule to implode and achieve ignition. One of the major sources of possible failure in ignition experiments is residual x-ray flux asymmetry on the capsule. All flux asymmetry can be analyzed in terms of the spherical harmonics Y_{lm}. If the flux is azimuthally symmetric (a good approximation in the NIF baseline cylindrical hohlraum illuminated by rings of beams), only the m=0 components exist and the flux asymmetry can be expressed in terms of the Legendre polynomials P_l and polynomial coefficients a_l.

Because the cylindrical hohlraum is symmetric about the midplane, odd Legendre modes are small in the absence of pointing errors and power imbalance. Because higher modes are smoothed out by radiation transport from the hohlraum walls to the capsule (with a transfer function that varies roughly as $\text{mode}^{-2.5}$ [2]), we are most concerned with diagnosing and controlling P_2 and P_4 flux asymmetry. Similar arguments have led researchers to study the low order symmetry modes in implosions driven by z-pinches as well [3].

Fig. 1 shows a typical NIF ignition capsules and the temperature drive profile. Four shocks keep the DT fuel on a low adiabat, so that the capsule may reach roughly 1000 g/cc at ignition time. The fuel must be compressed symmetrically to < 20% rms out-of-round over all modes < 10 to ensure such a high fuel density. Specifically, 2-D

integrated radiation-hydrodynamics simulations [4] show that the capsule will fail when the average flux Legendre coefficient a_l is greater than 1% of $a_{0,}$ since that leads by simple kinematics to a final rms core distortion (magnified by ≈ the 35x convergence ratio) of 35%/√(2l+1) out-of-round. Higher flux asymmetry modes such as a_6 have to be kept below 0.6% since they undergo additional hydrodynamic instability growth. Accounting for all other sources of target and laser imperfections, we have set the NIF specifications on intrinsic time-averaged flux asymmetry as a_2/a_0 and $a_4/a_0 < 0.25\%$ and the rms of all modes a_6 - $a_{10} < 0.5\%$ [5]. The time-dependent flux asymmetries can be somewhat higher and must average out to the values above. For example for the first three shocks of the drive pulse, asymmetries can be 2x larger, and for the first few ns, 5x larger than the time integrated values.

II. Asymmetry Diagnostics

A variety of different techniques can measure the symmetry in hohlraums using surrogate capsules. The reemission ball [6, 7] is a solid high Z (e.g. Bi) ball placed in the same central location as an ICF capsule. Thermal radiation on the ball heats up its surface, and it reemits as a blackbody at a slightly lower temperature, which will vary from point to point on the ball if the incoming flux is asymmetric. When viewed in for example hν = 1 keV x rays, the re-emission from the ball is highly sensitive to fluctuations around the characteristic 90eV foot NIF drive temperatures. Thus small variations in incident flux are amplified by a factor hν/4kTr, and can be measured as a function of time for the first 2 ns of the pulse before the re-emission ball surface expands and interacts with the hohlraum plasma.

A second asymmetry diagnostic is the x-ray imaging of imploded core shapes from a surrogate non-cryogenic capsule. The thickness of the capsule shell can be adjusted to vary the sampling time from full pulse down to the first ≈ 5 ns of the foot [8]. In this paper, we will concentrate on a mid-pulse symmetry diagnosis technique, the backlit imploding thin shell.

III. Thin shell asymmetry diagnostic

The thin shell diagnostic is a capsule having a thickness of 5-50% of the ignition point design capsule thickness to ensure an earlier acceleration and implosion time[3,9]. The shape of the imploding shell is interrogated by x-ray radiography after it has traveled ≈ 1/3 to 1/2 its initial radius. The backlighting source for the radiograph can be produced by different approaches, with the primary two techniques being point projection and areal backlighting both of which are studied in this work [10]. The dopant material (Ge for CH or Cu for Be) is also choosen to mimic the ignition target and the backlighter material and photon energy are choosen to match the capsule dopant with the dopant concentration modified to allow the radiographic contrast to be optimized. In addition, the thin shells can be fabricated with the outer 5 μm of the shell undoped to emulate the ablated material in the graded doped ignition point design capsules (see Figs. 1a and b) that is traversed by the inner cone of beams, hence emulating laser-plasma interaction conditions. Because the acceleration is proportional to the ablation pressure divided by the areal mass density $\int \rho dr$, and $\int \rho dr$ is approximately conserved during the implosion, the shape of the thin-shell capsule reflects the drive asymmetry [11].

We can increase the capsule/case ratio in the surrogate target to enhance the sensitivity to high-order flux asymmetries. Fig. 2 shows the radiation transfer function for a capsule within a spherical case for a capsule/case radii ratio of 0, 0.2, 0.4, and 0.6 in modes 0 through 8. Note that by increasing the capsule/case ratio from a NIF-like value of 0.4 to 0.6, the sensitivity to modes 6 and 8 are increased by an order of magnitude. The transfer function for a sphere inside a cylinder, the usual hohlraum shape, is more complicated because the Legendre polynomials and spherical harmonics are no longer the normal modes. However, when cross-coupling between modes is taken into account, there is still an order of magnitude increase in flux sensitivity to the higher modes with the higher capsule/case ratio. It should also be noted that Fig. 2 implies a strong reduction in transfer function as the shell implodes, which means that high order modes can best be measured just after shock break-out time.

IV. Experiments on the Omega Facility

Since the first proof-of-principle shots [9] we have run three sets of backlit thin shell experiments at the 60-beam Omega laser at the Laboratory for Laser Energetics at the University of Rochester. These experiments are designed to emulate the foot drive and candidate ablator materials of the NIF ignition target designs (see Fig. 1) while operating at close to NIF spatial scale to enhance detectability of shell distortions. The capsule-to-case radii ratios are chosen to be between 0.4 and 0.6 with the larger values having enhanced sensitivity to higher order modes ($>P_4$). Figs. 3a and b show the two

hohlraum irradiation and capsule geometries. The first experiments use a point backlighter [9,10] while the second and third sets use an area backlighter.

a) Point Projection Data:

The experimental geometry for the point projection radiography case is shown in Fig. 4. 3.3 mm-diameter by 5.8-mm-long Au hohlraums are driven by 5, 5 and 10 laser beams per ring per side at 21.4°, 42°, and 59° relative to the hohlraum symmetry axis (Fig. 3a). All 40 beams heat the hohlraum from 0 to 3.5 ns using a flattop drive, with nominally 240, 216 and 216 J per beam in the three rings entering each 2.07-mm-diameter laser entrance hole (LEH). A slightly larger 2.32 mm-diameter LEH was used for the hohlraum containing the largest shell (2 mm in diameter) to aid in alignment through the LEH. The intersection of the beams in each ring are on the hohlraum axis at 3.73, 3.42 and 2.69 mm, respectively from hohlraum center, and each f/6.6 beam is defocused by -2.07, +0.73 and +2.07 mm with respect to the intersection point, where negative values refer to focussing beyond the intersection point. The cone pointing and energies per cone were chosen to provide a symmetric drive for the case of the smaller LEH. The average hohlraum drive,measured through one LEH at 37.4° to the hohlraum axis by a multichannel soft x-ray diode array ("Dante") [12]), reaches 100 eV reproducibly after 3.5 ns (see Figure 5).

At the center of each hohlraum is placed a 12 μm-thick 3.4% uniformly Ge doped CH shell of 1.1 g/cc. The shell outside diameter is varied between 1.3 and 2 mm to provide capsule-to-case radii between 0.4 and 0.6. To create the 4.7 keV Ti He α x-ray

backlighter, six other 3.5 ns, 240 J beams are delayed by 4 ns and focused to a 500 μm-spot onto a Ti disc at 0.5 mm from a 50 μm pinhole drilled in 100-μm-thick Ta [10]. The pinhole itself is 7 mm from the shell, projecting a single 15.6x magnification radiograph of the imploding shell through viewports on the hohlraum midplane onto a single-strip gated MCP-based framing camera at 10 cm. The MCP is filtered with 500 μm Be and 25 μm Ti to reduce both soft and hard x-ray backgrounds. It is triggered at 5.4 ns using a 240 ps gate, long enough to provide adequate photon collection yet short enough to avoid significant motional blurring of the shell, thathas reached an inward velocity of about 100 μm/ns at that time. Unlike prior experiments, the viewports on the hohlraum are covered with just 50 μm CH rather than a thin high albedo, high Z inner coating on CH to avoid previously observed non-uniform transmission ascribed to break-up of the high Z patches due to hydrodynamic instabilities.

Fig. 6 shows three radiographs of initially 1.3, 1.6 mm, and 2 mm, 15 μm-thick CH(Ge) shells taken at 5.4 ns after a travel distance of 220-240 μm. The limb positions are analyzed as a function of angle (see later discussion) and fitted to a Legendre polynomial for all modes up l = 10. Fig. 7 plots the extracted Legendre coefficients in μms for the three different initial capsule sizes, normalized to the average distance travelled. One can see a statistically significant and expected increase in sensitivity to medium modes (3, 4, 5 and 7) between the largest and smallest capsule, corresponding to less hohlraum drive smoothing. For example, accounting for coupling between a cylindrical hohlraum of about this aspect ratio and spherical shell, the expected [13] increase in P_4 sensitivity between a 1.3 and 2 mm shell is 3x, in agreement with the data. For the lowest P2 mode, one expects only a 30% increase in sensitivity between 1.3 and 2

mm shells, while the data appears to show a drop in sensitivity. The more positive value in a_2 for the largest shell can be largely ascribed to its 30% larger LEH leading to a calculated [14] 4% more negative value of drive P_2 relative to P_0, hence 4% more positive thin shell distortion a_2 relative to a_0. Higher modes are much less affected by changes in LEH size. Overall, the a_2 distortion is more negative than expected, corresponding to less drive on the hohlraum equator thus creating oblate shell (see Figures 6a and b), suggesting less inner beam first bounce coupling than expected, consistent with results discussed in the later area backlighting section. Fig 8 plots the extracted Legendre coefficients in μms for two nominally identical initially 1.6 mm shells driven by the solid and dashed drives shown in Figure 5. The reproducibility is within error bars, and suggests initial shell thickness or areal density non-uniformities are < 1%.

The error in a specific Legendre mode, σ_l, due to a random limb radius measurement error per line-out σ_{rms} is given by

$$\sigma_l \equiv \frac{\Delta a_l}{a_0} \approx \frac{\sqrt{2l+1}\,\sigma_{rms}}{d\sqrt{n}} \qquad (1)$$

where n is the number of independent radial line-outs and d is the distance traveled by the shell. The $\sqrt{2l+1}$ term arises from the fact that the Legendre mode P_l has an rms of $1/\sqrt{2l+1}$. In our experiments on Omega, $\sigma_{rms}$is typically 4 μm for n = 50. Thus, for d = 200 μm, the random error for a given Legendre coefficient a_l/a_o is $\sqrt{2l+1}$ 0.3%.

The fitting error bars of ± 1% in $a_{2\text{-}4}$ shown in Figs. 7 and 8 for 220 μm travel are consistent with this estimate. They extrapolate to ± 0.3% accuracy for 700 μm travel expected of full scale tuning targets (1.1-1.2 mm initial radius), well within the 0.5% symmetry control requirement for the foot of the pulse.

b) Area Backlighter Data

A second set of experiments studied Cu doped Be thin shells with an area backlighter (Fig. 9) in a hohlraum with a NIF-like case to capsule radius ratio of 0.39 and with a hohlraum and shell diameter that were 70% of the values for a NIF ignition design (scale 0.7). The spherical shell is 15 μm-thick, comparable to the thinnest shell design for ignition experiments, with greatest sensitivity after shock break-out occurring at 0.4 ns. The outer 5 μm are pure Be to best emulate the plasma conditions at the surface of the ablator in a pure Be ignition target design, while the inner 10 μm are doped with 2% Cu to increase the contrast of the absorption limb produced by the shell at the 4.7 keV Ti backlighter energy to an optimal value of minimum transmission that is near 50%. The cylindrical Au hohlraum shown in Figure 3b was illuminated with a 1 ns square pulse for both drive and backlighter beams, which was chosen to give the brightest backlighter and highest measurement quality, while maintaining a peak drive just above 100 eV to emulate the first two ns of a full scale ignition design. The drive beams are arranged in an inner cone on either side (eight beams per side) with a cone half angle of 23° and an outer cone on either side (10 beam per side) with a 48° half angle as shown in Figure 3b. The drive beams on the small angle (inner) cone have their best focus spot size maintained at 640 μm FWHM by a distributed phase plate (DPP), while the large angle (outer) cone beams are unsmoothed and defocused. The hohlraum also has a 1350 μm diameter hole in the wall covered with a Ti patch (12.5 μms thick) that is illuminated by

six backlighter beams arranged in a circle of 250 μm radius with DPP smoothed spots of 800 μm FWHM and two additional beams that were defocused and covered the entire foil. This provided a uniform source of x-rays over the 760 μm diameter circle corresponding to the converged shell size at the exposure time. The opposite side of the hohlraum also has a 1350 μm diameter hole cut to allow the x-ray camera to have an unattenuated view of the 4.7 keV x rays that are generated on the Ti foil and transmitted through the shell.

The experiments investigated three different illumination configurations to verify the sensitivity of the measured shell distortion to an imposed l =2 mode perturbation in the incident laser power. Specifically, shots 49739, 49741 and 49740 varied the inner cone energy fraction from 0.30 to 0.33 to 0.38, while the total drive energy was 9.70, 11.3 and 9.86 kJ, respectively. The shells were imaged with four separately timed micro-channel plate (MCP) strips of an x-ray framing camera, each of which had four images taken within 180 ps of each other to produce a total of 16 images for each experiment as shown in Fig. 10a. The framing camera produced these images with a 4 x 4 array of 20 μm pinholes set-up to produce a 4x magnification of the image plane at the shell when projected to the detector plane. The instrument was filtered with 25 μm of Be to separate the 4.7 keV Ti backlighter line from thermal x-rays at lower energy. The four strips were timed to capture images when the ball had converged to a little more than 1/2 its initial radius of 700 μm, with the average time of the four different images on each of the four strips set at 6.9, 7.15, 7.4, and 7.65 ns after the start of the drive pulse.

Figure 11 shows the x-ray drive measured on these three shots [12]. The drive increases with the incident laser energy but is fairly insensitive to the fraction of the energy in the inner cone, as expected.

In addition to the errors introduced by the statistical error in the camera discussed earlier, another source of error, backlighter non-uniformity is also considered. Radial gradients in the emission behind the absorbing shell can produce distortion in the backlit image that is not present in the shell itself. .To correct for non-uniformities, we used a second x-ray framing camera viewing the back of the backlighter foil at an angle of 44° off normal, which is shown in Fig. 12. The measured backlighter profile shows little evidence of the structure produced by the six overlapping spots, suggesting that the volume emission of the expanding plasma and the associated electron heat transport are effectively smoothing the x-ray emission profile and leaving primarily relatively large scale structure and radial gradients as seen in Figure 12. The effect of the backlighter structure is removed from the image of the shell by stretching the backlighter image to compensate for the off-normal view angle and then dividing the shell image by the corrected backlighter image. This is done for each shell image, using the separate image of the backlighter taken from the same frame on the backlighter viewing camera. These corrected images have been analyzed to produce measurements of the average radius and the dependence of the radius on angle (distortion) by a process of identifying the radial location of the minimum of transmission as a function of angle from the hohlraum symmetry axis, and separating the measured distortions into Legendre modes. To illustrate this process we discuss in detail each step in the data analysis on the third strip (7.4 ns) for each of the three experiments, as indicated in Figure 10a, and then present the

final results of the analysis for all strips. From the array of 16 images, each individual image is removed (examples shown Figs. 10b, c and d) and analyzed separately. Inspection of the three images immediately reveals that shot 49739 shows the shell is flattened somewhat at angles close to the axis of the hohlraum, which is indicated with an arrow in Figure 10b, whereas shot 49740 is closest to circular, indicating the sensitivity of the ball shape to the change in l =2 component of the laser drive. Shot 49741 shows a reduced capsule radius relative to the other two shots in response to the increased drive energy on this shot, as well as a l = 2 distortion that is intermediate to the first two shots as expected from the intermediate value of cone fraction.

A precise measurement of these effects is provided by computational analysis of the images shown, which is discussed in the appendix. The average radius of each shell from each strip of four images at t = 7.4 ns is shown in Figure 13, with error bars representing the standard error of the mean of each of the four images. This data clearly demonstrates that the expected trend of reduced shell radius with increased drive is well within the accuracy of the measurement. The data also demonstrates both good reproducibility of the radius measurement, and little dependence of the average radius on the cone fraction at low drive. The residual radius variations vs. angle from a single strip are shown in Figure 14 for shots 49739 and 49740. Figure 14a shows clearly the largest values of the radius being near $\theta = 90°$ and 270° (0° corresponds to the hohlraum axis) as expected since the fraction of laser power driving the shell near $\theta = 90°$ is less due to the lower inner cone fraction on this shot. The figure also shows that the variation of the lowest mode perturbations from image to image on the same strip is less than the average size of the perturbation indicating that these distortions are well above the measurement

error. The limb radii vs. angle are then used to get quantitative information about the first 10 Legendre modes by performing a Legendre transform on each and calculating the four image average of each of the first 10 mode amplitudes. The resulting 10 distortion modes and their standard errors are shown for each of the three shots in Figure 15. Again the l = 2 component is the dominant mode when the cone fraction is low and the variation of the l = 2 component with cone fraction is apparent. In this data the l = 1 component is removed in the analysis. Higher order modes can be affected by backlighter non-uniformity. For example, the ordering of the l = 3 component vs. shot is consistent with the observed shift of the backlighter centroid with respect to the shell centroid along the hohlraum axis as shown in figure 10. The amplitudes of higher mode numbers are not significantly greater than the measurement error, with the exception of a significant mode 6 in one shot and mode 7 in another. In both cases the magnitudes are consistent with the expected structure in the partially-overlapped multi-beam backlighter in those modes at that radius.

To best relate the measured distortion to the drive symmetry we take the ratio of the mode distortion of the shell to the average distance traveled by the shell between the beginning of the drive pulse and the time of the image. The normalized l = 2 mode distortion measured both before and after the backlighter profile is removed is shown in Figure 16. The mode amplitude in the corrected image relative to the uncorrected image is comparable to the statistical error. Note that the measured, normalized = 2 component is found to be quite linear with the cone fraction, as expected, providing us with a verification of the sensitivity of the thin shell technique for measuring drive symmetry in an ignition relevant hohlraum with a Be ablator material.

A similar analysis was applied to all high quality images taken during the 1 ns backlighter pulse, which includes two images on the strip timed at 6.9 ns, and four each on strips timed at 7.15 ns, and 7.65 ns in addition to the images from 7.4 ns discussed above. The data show the expected shell inward velocity and slow change in distortion over this brief time period. The results of this first series of experiments are compared with 2D simulations of the hohlraum and thin shell that use the experimentally measured laser drive. The simulations model the backlighter port and diagnostic viewing hole with a radiation loss term near the waist of the hohlraum, and model the shell as a uniform layer of mixed Be and Cu with the total amounts of each equal to the experimental values. The simulated conditions in the hohlraum are then post-processed to produce a simulated x-ray image as shown in Figure 17 a) by integrating the x-ray absorption of the 4.7 keV Ti line produced by the backlighter, over the line of sight of the camera at each point in the image. The result is an image of x-ray transmission from which line outs are taken to determine the absorption limb along different slices through the image as shown in Figure 17 b). The minimum of transmission points are used to determine the radius of the shell at each time considered as well as the $l = 2$ component of the shell distortion. These simulated values of r and a_2 are shown compared to the measured values in figures 13 and 16, where it is seen that the measured radii at low drive are close to the simulated values and the high drive measurements of radius are somewhat larger. In addition the measured a_2 is consistently more negative than the simulated value, consistent with the earlier point projection results and re-emit data [7],suggesting that the x-ray drive produced by the inner cone of beams is less than expected as could be caused a number of effects not modeled, including reduced early time inner cone x-ray conversion

efficiency, or power transfer between the crossing beams by ion wave stimulated in the flowing plasma, the study of which is on-going and outside the scope of this paper. Nevertheless, the simulated rate of variation of a_2 as cone fraction is changed is similar to the observations indicating that the thin shell technique has the expected sensitivity to drive asymmetry for the $l = 2$ mode. Moreover, the ±0.5% $l = 2$ accuracy averaged over 4 frames demonstrated for 350 μm of travel extrapolates to ±0.25% accuracy for full NIF-scale targets, again meeting ±0.5% requirements.

A third series of experiments with Cu doped Be thin shells was carried out with a longer, reverse ramped, laser pulse to better emulate the several ns duration planned for the foot of the pulse in ignition experiments. The advantage of the longer pulse is a higher drive at late time to better emulate the ignition foot, which trades off against the lower peak drive, and lower peak brightness of the backlighter. As a result, this configuration is the best emulation of the drive conditions and is used to test the integrity of the thin shell throughout a long x-ray drive pulse. The hohlraum was identical to that shown in Figure 3b, except the laser entrance holes (LEHs) were reduced to 1780 μm diameter to maintain high drive temperature by reducing losses. The thin shell capsule was also made of Cu doped Be similar to that shown in Fig. 3b with a reduced total shell thickness of 12.4 μm (3.8 μm of pure Be for the outer layer and 8.6 μm of Be doped with 2% Cu for the inner layer) to maintain distance traveled with reduced drive energy. The laser power pulse was the same on all beams and ramped up to maximum power in 250 ps, and maintained there until 750 ps at which point the power ramps linearly down to 1/3 of the maximum at 3.5 ns then drops to zero in ~ 200 ps.

The converging shell driven by the reverse ramped pulse, is imaged by the x-ray framing camera as set up for the experiments shown in Fig. 9, but with an increased gain setting on the MCP to accommodate the reduced backlighter power. The timing of the four strips was spaced out to cover the length of the backlighter pulse and the desired image of the shell converged to a radius of 370 μm was obtained at 7.68 ns. Because of the lower backlighter intensity the x-ray brightness dropped off rapidly in the radial direction. An image from a separate experiment was taken with the backlighter and camera timed before the shell had converged to less than the 675 μm radius of the viewing hole, which provides a measure of the backlighter uniformity with little spatially dependent attenuation in the field of view. The ratio of azimuthally-averaged line-outs (Figure 18a) from these two images, together with a small correction for the attenuation of the un-converged shell and the shot to shot variation of the energies in the backlighter beams, provides a direct measure of the transmission of the shell as shown in Fig. 18 b. For r > 400 μm the measured transmission also approaches the expected value of 1 but has large fluctuations due to the fact that raw signals are both becoming small and photon noise in the data has a large effect on the ratio. The narrow, well defined feature near the transmission minimum indicates that the absorbing material has maintained its original spherical shell structure even after it has converged to nearly 50% of it initial size, consistent with requirements for NIF symmetry tuning and expectations [11].

The observed transmission limb thickness and radius has been compared with 2D simulations [15] as shown in Figure 19. The simulations used the as measured energies in the drive beams and also modeled the diagnostic hole as a loss term near the mid plane of the hohlraum. We find excellent agreement in the width of the limb, and the radius of

minimum transmission, as well as good agreement with the measured values of transmission. These results suggest the integrity of the thin shell surrogate target under ignition like drive conditions is maintained for 0.5x convergences. .

VII. Conclusions

Our OMEGA experimental campaigns have developed the thin shell diagnostic for use on NIF with the needed accuracy of better than 0.5% flux asymmetry measurement for the first 6 modes. The thin shell diagnostic has the advantage of linearity over alternative measurement techniques, so low-order modes will not corrupt the measurement of high-order modes. It also has the advantage over foam ball techniques in that the thin shell can be constructed with the planned ablator materials. Both point projection and area backlighter radiography have been validated. The results show the expected sensitivity to case-to-shell ratio and sufficient reproducibility, validating the uniformity of shell fabrication. Further we have designed experiments with Be thin shells to verify the sensitivity of the measurements to P_2 modes, and demonstrated the integrity of the thinnest practical shells envisaged after they have converged the required 50% of their initial radii. These thinnest shells provide sensitivity as early as 1.5 ns into the foot of the ignition drive pulse, hence overlapping with the reemission technique good to 2 ns.

Appendix on Image Analysis with Area Backlighters

The analysis of the images studied in the section proceeds by first identifying the center of the shell, then averaging over the 360° angle (with 0° corresponding to the axis of the hohlraum) to produce an angularly averaged function of signal vs. radius, from which a value of the radius of minimum signal is determined and reported as the shell radius at the time of the image. For the area backlighting, this process is repeated for each of the four images on the strip, which because of their close proximity in time (within ± 90 ps of the average time) and close proximity in viewing angle (within a cone of 3°), are treated as independent measurements of the same object and used to generate statistics on errors produced by camera noise, photon noise, and any rapidly time varying backlighter non-uniformity, to provide a measure of accuracy. The rms, or standard deviation, of the radii is divided by the square root of the number of images (or 2 in this case) to produce an estimate of the standard error of the mean of the four measurements which is used as an error bar representing measurements errors produced by the detector.

From the angularly averaged signal function, the region of the minimum is extracted, keeping radii that have signals up to ~ ½ of the maximum value on each side of the minimum. This region of limb minimum is then correlated with 500 image slices at 0.7° wide, equally distributed over 360°. The shift in radius scale for each slice that provides the maximum value of the correlation is reported as the deviation in radius vs. angle.

Acknowledgements

We thank the Laboratory for Laser Energetics, University of Rochester, for the use of the

OMEGA laser.

This work was performed under the auspices of the U. S. DOE by Lawrence Livermore National Laboratory under Contract No. DE-AC52-07NA27344. LLNL-JRNL-406419

References

[1] J.D. Kilkenny, T.P. Bernat, B.A. Hammel et al, Laser and Part. Beams **17**(2), 159-171 (1999), and J.D. Kilkenny, E.M. Campbell, J.D. Lindl et al, Phil. Trans. Royal Soc. of London **357**(1752), 533-553 (1999); and J.A. Paisner, J.D. Boyes, S.A. Kumpan, W.H. Lowdermilk, M.S. Sorem, Laser Focus World 30, 75 (1994).

[2] S.M. Pollaine, Nuclear Fusion 40, 2061 (2000).

[3] R. A. Vesey, M. E. Cuneo, G. R. Bennett, J. L. Porter, Jr., R.G. Adams, R. A. Aragon, P. K. Rambo, L. E. Ruggles, W.W. Simpson, and I.C. Smith, Phys. Rev. Lett. 90, 035005-1 (2003), G. R. Bennett, M. E. Cuneo, R. A. Vesey, J. L. Porter, R.G. Adams, R. A. Aragon, J. A. Caird, O. L. Landen, P. K. Rambo, D. C. Rovang, L. E. Ruggles, W.W. Simpson, . C. Smith, and D. F.Wenger Phys. Rev. Lett. 89, 245002-1 (2002), Roger A. Vesey, Michael E. Cuneo, John L. Porter, Jr., Richard G. Adams, Rafael A. Aragon, Patrick K. Rambo, Laurence E. Ruggles, Walter W. Simpson, Ian C. Smith, Guy R. Bennett, Physics of Plasmas, 10,1854 (2003).

[4] G.B. Zimmerman and W.L. Kruer, Comments Plasma Phys. Control. Fusion 2, 51-61 (1975).

[5] S.W. Haan, private communication.

[6] N.D. Delamater, G.R. Magelssen and A.A. Hauer, Phys. Rev. E 53, 5240 (1996).

[7] E. Dewald, et al. to be published in Rev. Sci. Inst. (2008).

[8] A. Hauer, N. Delamater, D. Ress et al., Rev. Sci. Instrum. 66, 672-7 (1995); and N. D. Delamater, T. J. Murphy, A. A. Hauer et al., Physics of Plasmas 3, 2022-8 (1996); R. Turner, P. Amendt, O.L. Landen, S.G. Glendinning, P. Bell, C. Decker, B.A. Hammel, D. Kalantar, D. Lee, et. al., Physics of Plasmas 7, 333-337, (2000).

[9], S. M. Pollaine, D. K. Bradley, O. L. Landen, R. J. Wallace, O. S. Jones, P. Amendt, L. J. Suter, and R. E. Turner, Phys. Plasmas 8, 2357 (2001).

[10] D. K. Bradley, O. L. Landen, A. B. Bullock, S. G. Glendinning, and R. E. Turner Opt. Lett 27, 134 (2002), O. L. Landen, D.R. Farley, S.G. Glendinning, L.M. Logory, P.M. Bell, J.A. Koch, F.D. Lee, D.K. Bradley, D.H. Kalantar, C.A. Back, and R.E. Turner, Rev. Sci. Instrum. 72, 627 (2001).

[11] Peter Amendt, A. I. Shestakov, O. L. Landen, D. K. Bradley, S. M. Pollaine, L. J. Suter, and R. E. Turner, Phys. Plasmas, 8, 2908 (2001).

[12] H.N. Kornblum, R.L. Kauffman, and J.A. Smith, Rev. Sci. Instrum. 57, 2179 (1986); K. M. Campbell, F. A. Weber, E. L. Dewald, S. H. Glenzer, O. L. Landen, R. E. Turner, and P. A. Wade, Rev. Sci. Instrum. 75, 3768 (2004).

[13] J. Lindl et. al., Physics of Plasmas **2**(11), 3933-4024 (2003).

[14] O. L. Landen, P. A. Amendt, L. J. Suter, R. E. Turner, S. G. Glendinning, S. W. Haan, S. M. Pollaine, B. A. Hammel, M. Tabak, M. D. Rosen, and J. D. Lindl, Phys. Plasmas 6, 2137 (1999).

[15] M. J. Schmitt, S. R. Goldman, to be published.

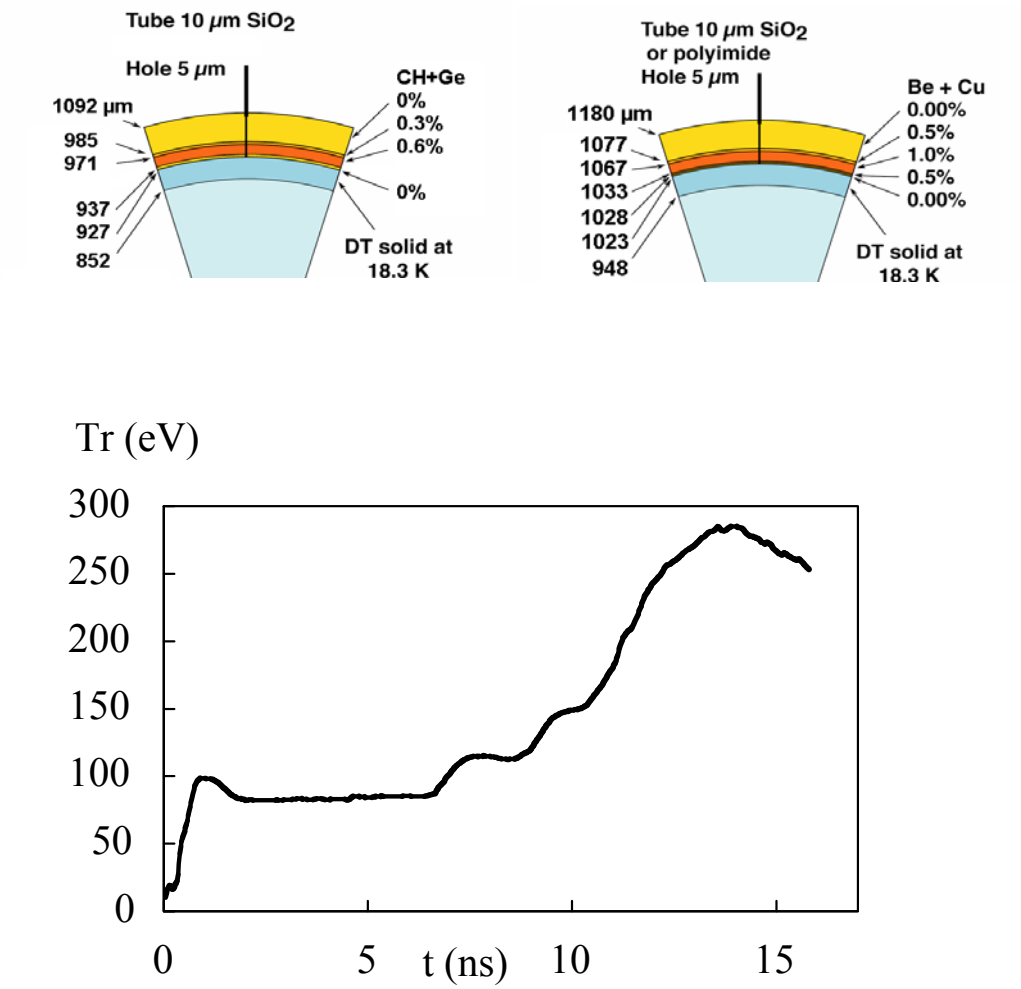

Figure 1 Designs of ignition capsules a) CH(Ge) and b) Be(Cu). C) Radiation drive vs time for the Be(Cu) case showing 4-shock structure where foot of pulse ends at ≈ 10 ns.

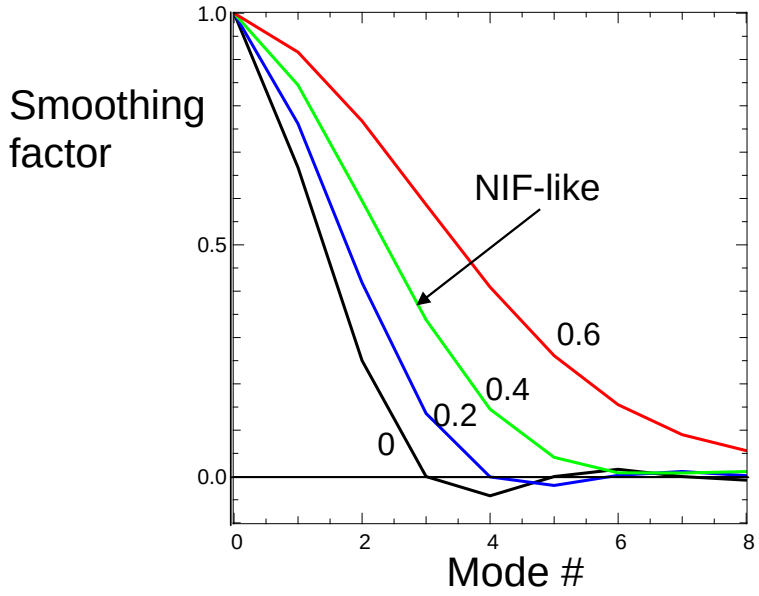

Figure 2 Ratio of asymmetry at capsule vs asymmetry at hohlraum wall ("smoothing factor") vs asymmetry Legendre mode number for various ratios of capsule to hohlraum initial radii.

a)

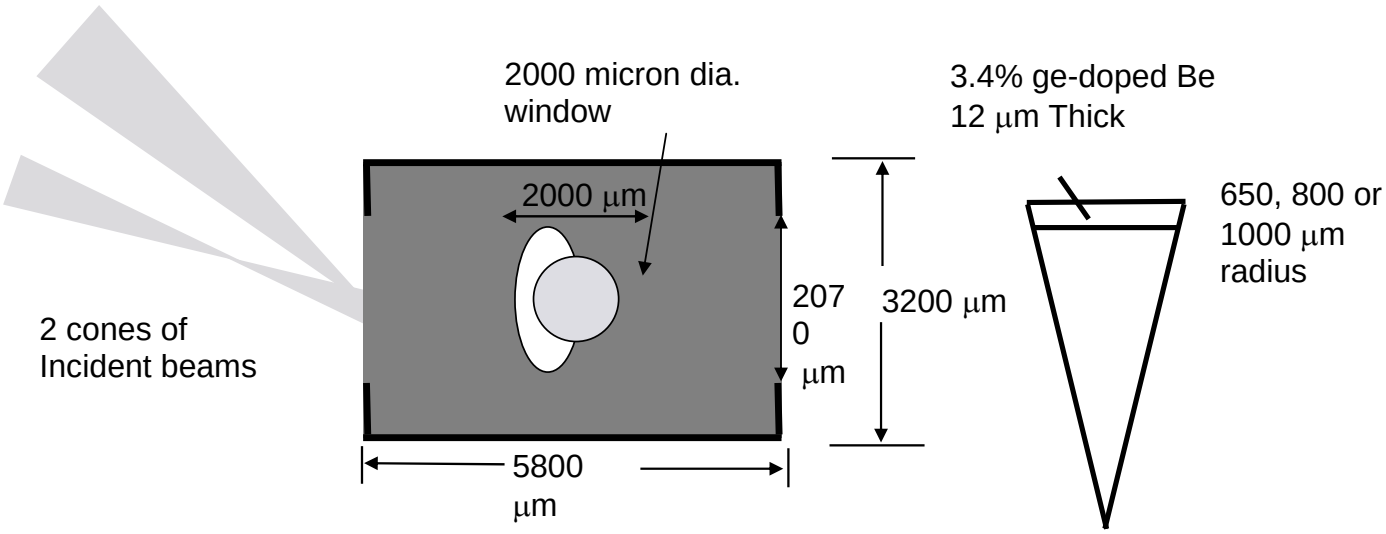

b)

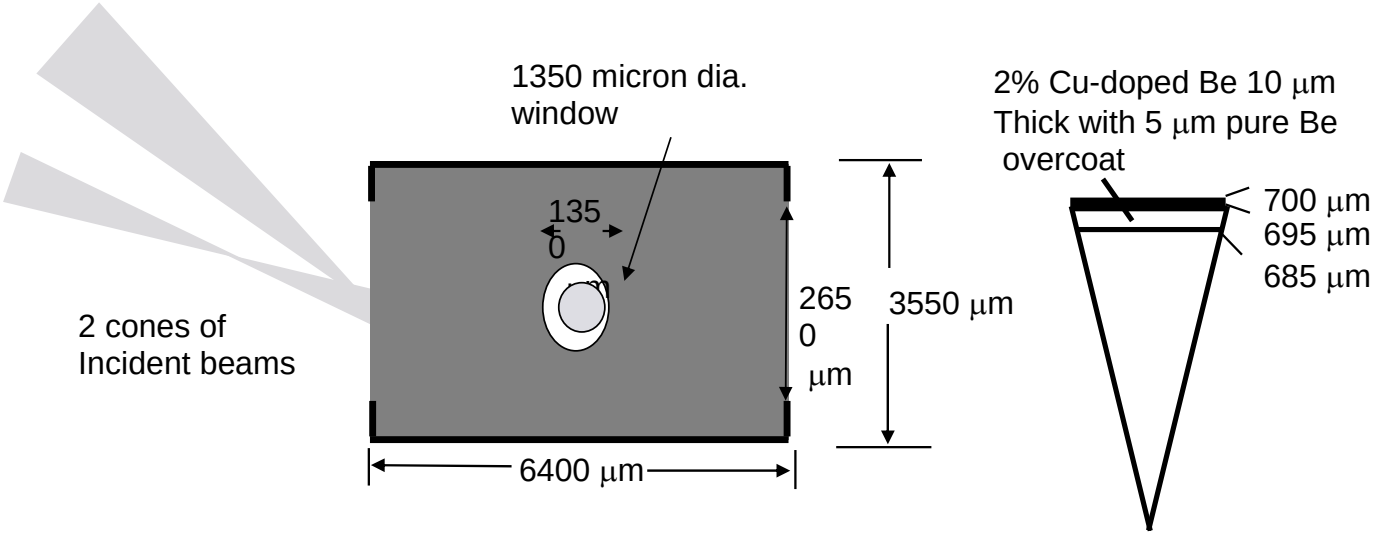

Figure 3 a) The Omega CH(Ge) hohlraum and shell design b) The Omega Be(Cu) hohlraum and shell design.

Comment [L1]: Put beams drawn to sacle in hohlraum figures.

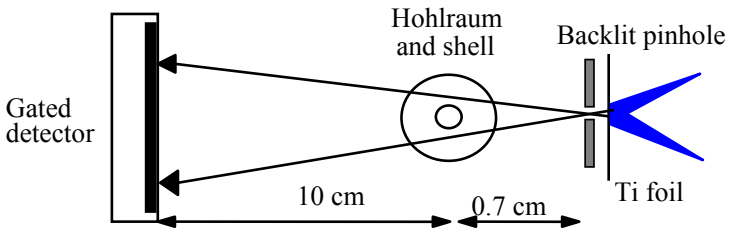

Fig. 4 Experimental geometry for point projection radiography

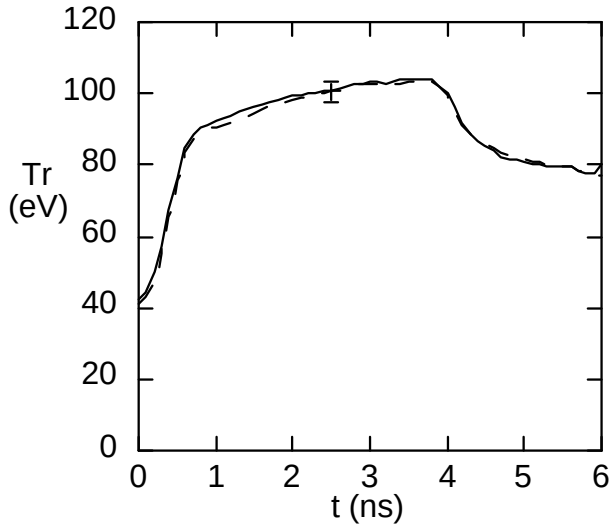

Figure 5. Measured soft x-ray radiation drive vs time for two nominally identical hohlraum shots equipped with 1.6 mm diameter shells. Error bar represents absolute systematic error.

a) b) c)

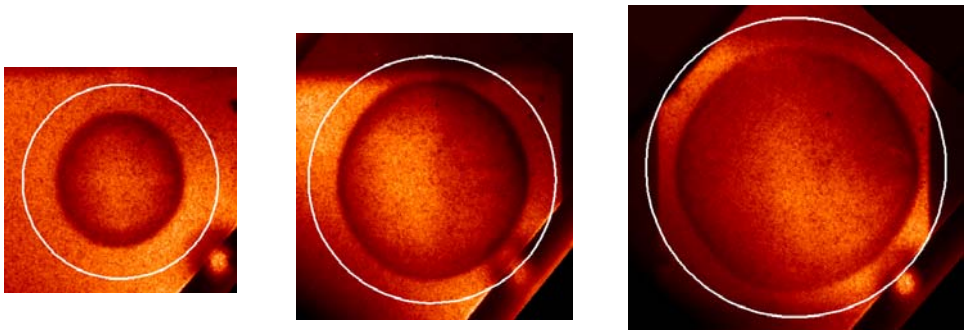

Figure 6 4.7 keV point projection radiographs of initially a) 1.3 mm, b) 1.6 mm and c) 2 mm-diameter, 15 μm-thick CH(Ge) shells. The hohlraum axis is horizontal and the white circles denote initial shell size.

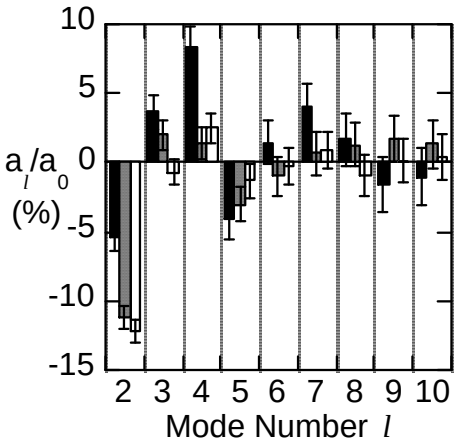

Figure 7 Legendre mode amplitude normalized to distance travelled (a_0) for the 2 mm shell (black bars), 1.6 mm shell (gray bars) and 1.3 mm shell (white bars) data shown in Fig. 6.

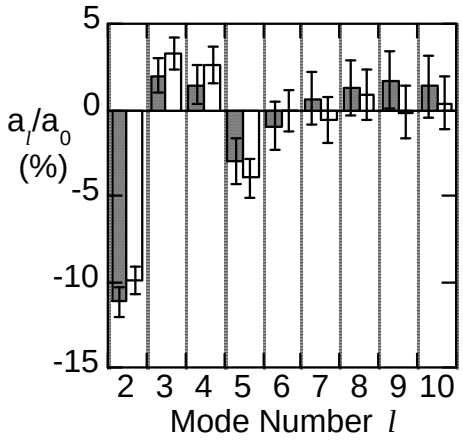

Figure 8 Comparison of Legendre mode amplitude normalized to distance travelled (a_0) for two shots with nominally identical drive and shell parameters (1.6 mm initial diameter).

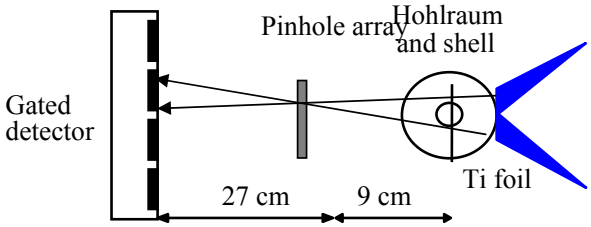

Figure 9 Experimental geometry for area radiography

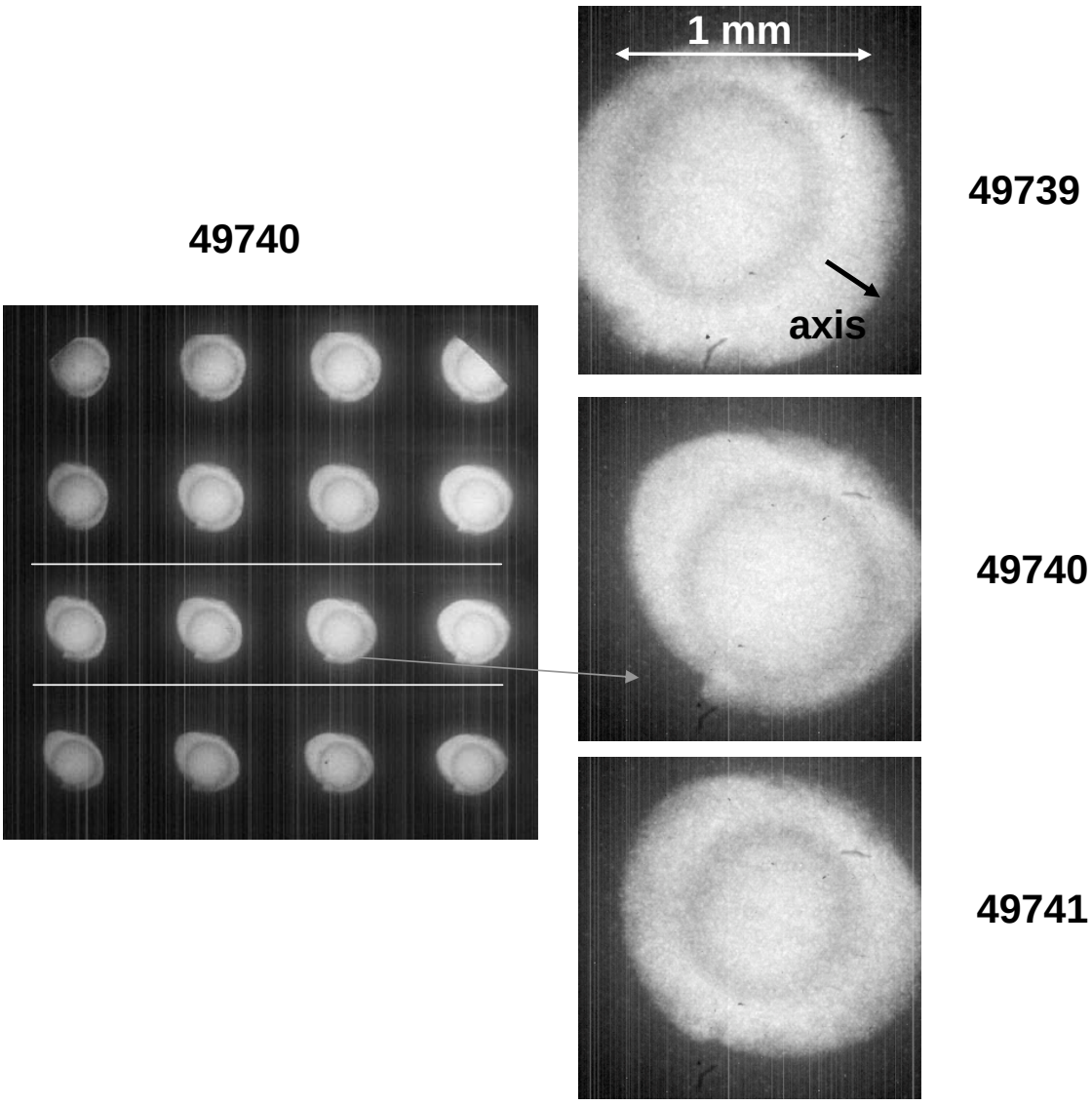

Figure 10 a) Gated x-ray images of the backlit shell, at times 6.9, 7.15, 7.4, 7.65 ns. b), c) and d) Magnified images at time 7.4 ns of the three shots

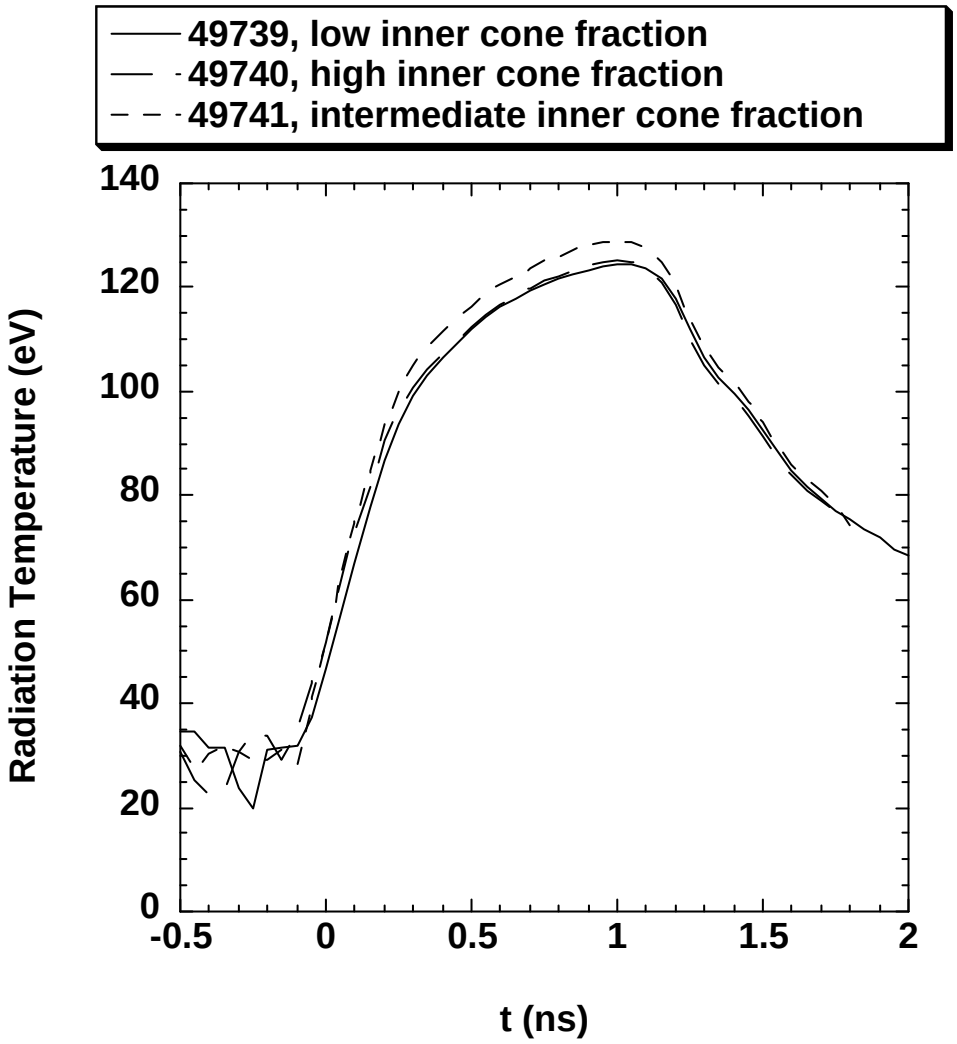

Fig. 11 Measured drive temperature through LEH vs. time for the three shots.

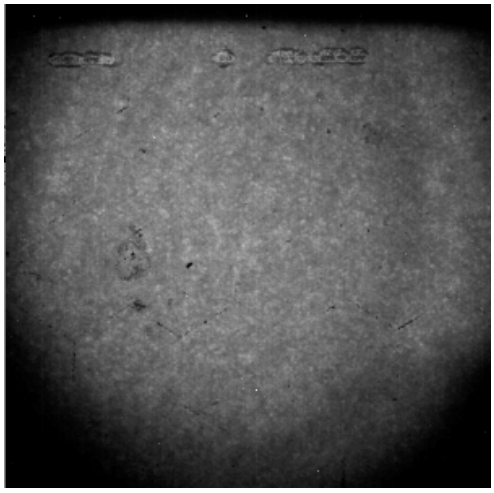

Figure 12 Example of x-ray image of backlighter as viewed from the back side at a 44° incidence angle.

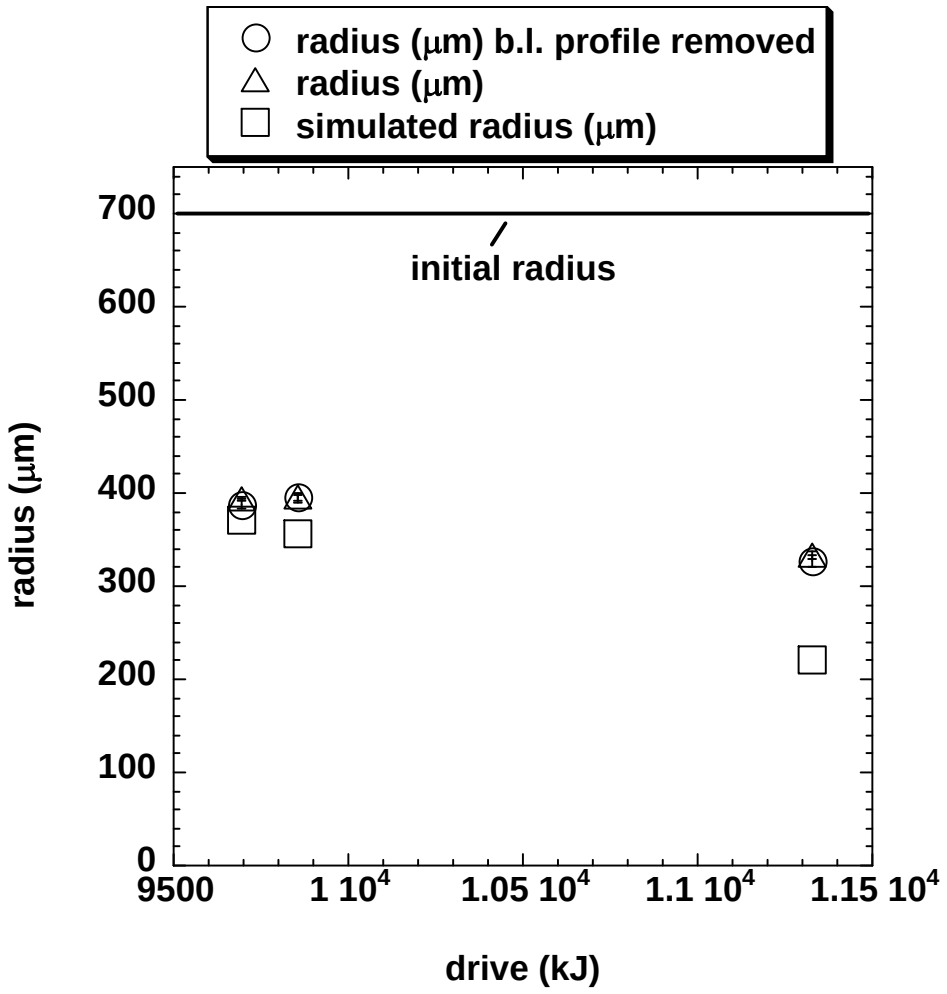

Figure 13 Measured vs calculated average radius of the shells with (dots) and without (triangle) the effect of backlighter non-uniformity removed.

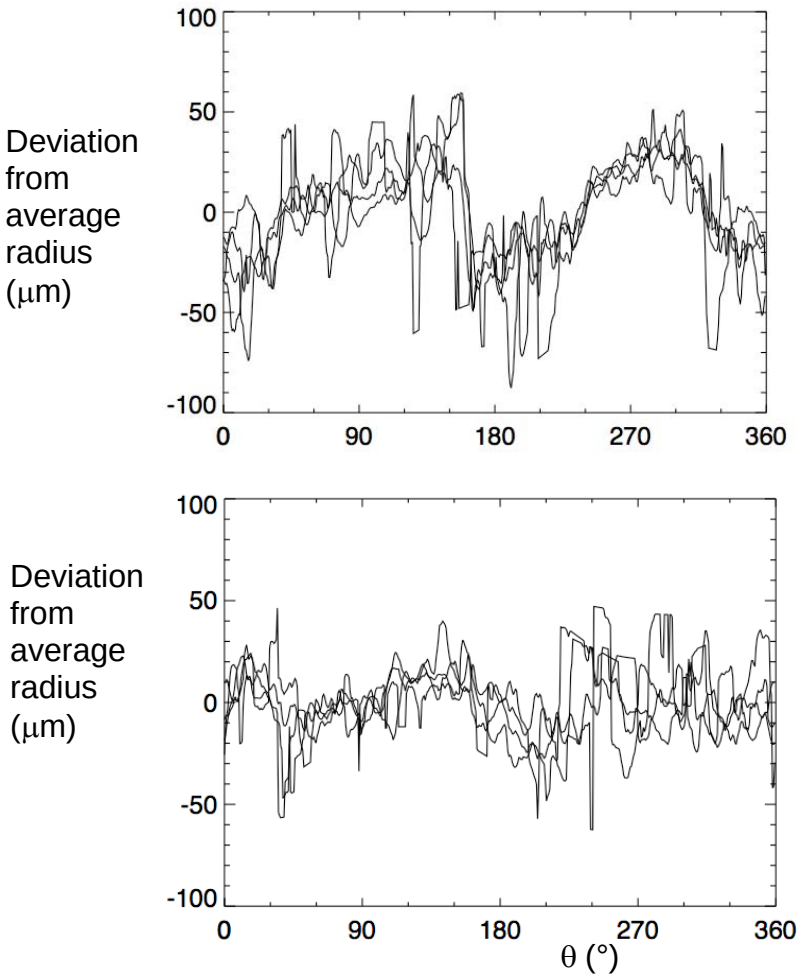

Figure 14 Deviation of limb radius from average radius vs. angle for each of four images on same 7.4 ns strip for a) Shot 49739 and b) Shot 49740.

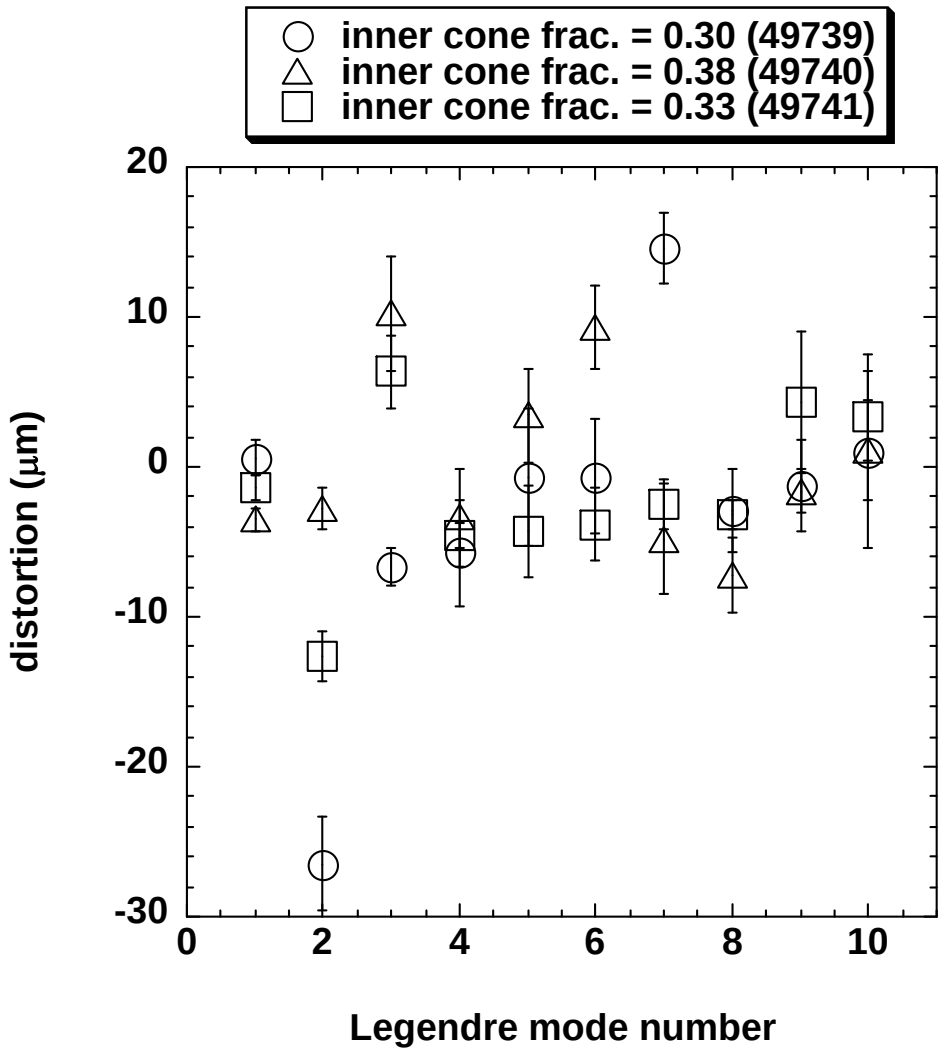

Figure 15 Legendre mode amplitudes vs mode number for inner cone fractions 0.3 (dots), 0.33 (squares) and 0.38 (triangles) with the error bars representing the standard error of the mean of the four images from each experiments.

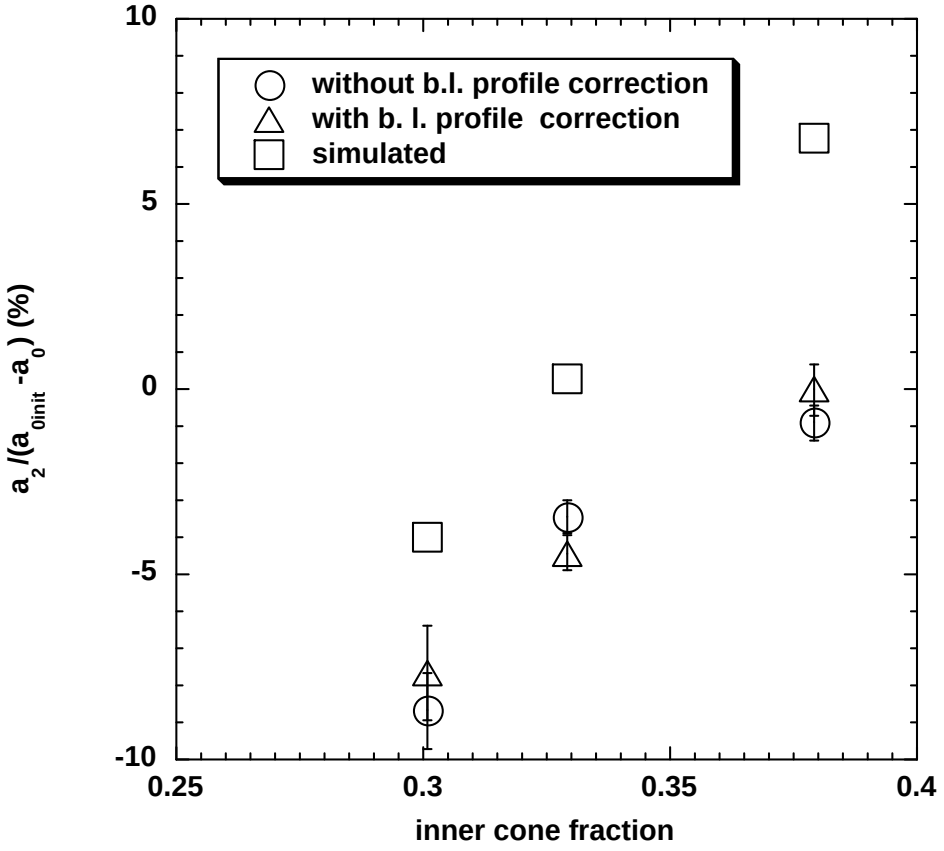

Figure 16 Measured vs calculated $l = 2$ mode distortion as percentage of average distance traveled vs inner cone fraction, with (triangles) and without (dots) the effect of backlighter non-uniformity removed.

Comment [L2]: This needs simulations added.

a)

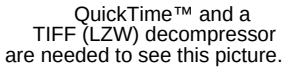

b)

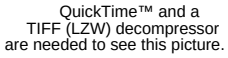

Figure 17 a) Example of backlit simulation of the converged thin shell and transmission at different times.

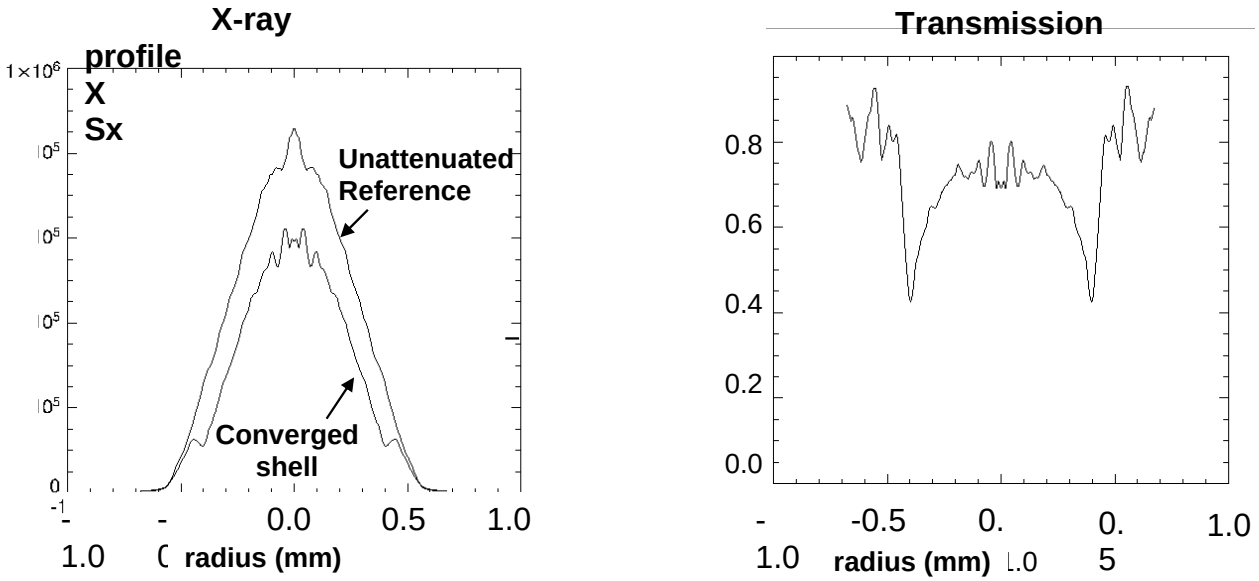

Figure 18 a) Angularly averaged reference and x-ray transmitted line-out of the backlit Be thin shell b) Ratio of transmitted to reference line-out

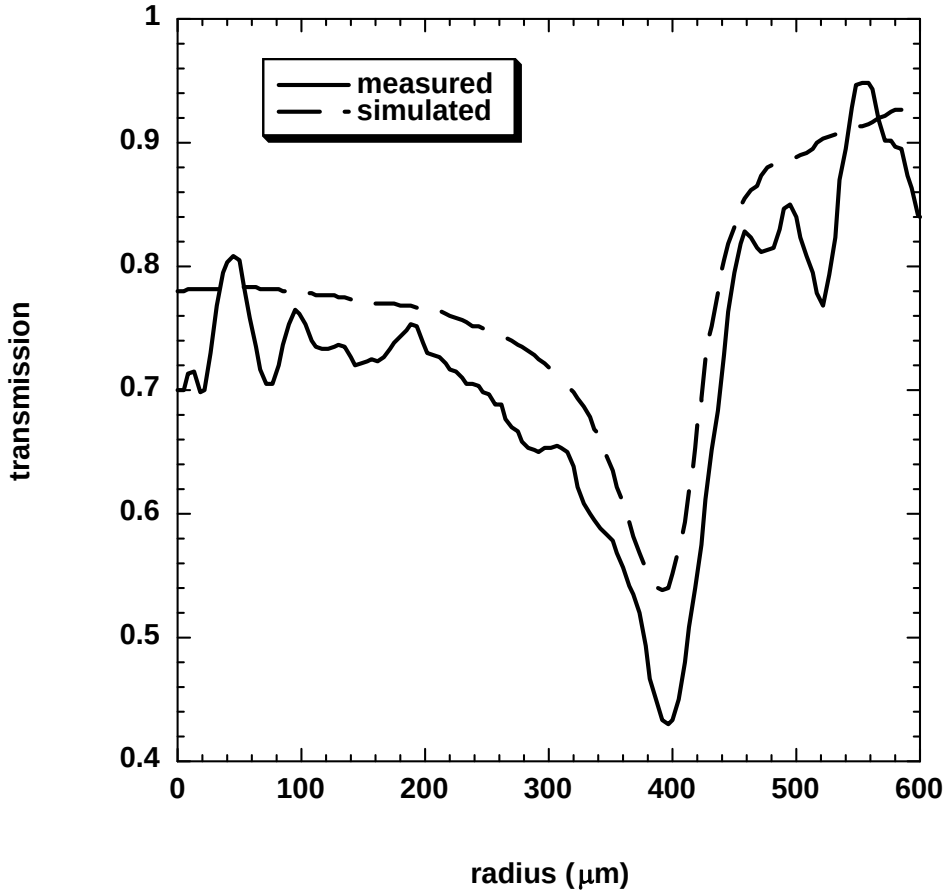

Figure 19 Comparison of measured vs calculated transmission limb